A Volumetric Integral Radial Basis Function Method for Time-Dependent Partial Differential Equations: I. Formulation

E. J. Kansa*, H. Power†, G. E. Fasshauer‡, L. Ling §

Abstract

A strictly conservative volume integral formulation of the time dependent conservation equations in terms of meshless radial basis functions (RBFs) is presented. Rotational and translational transformations are considered that simplify the partial differential equations (PDEs) to be solved. As a result, the solutions that are represented at a finite sample of knots, $x \in \Omega \setminus \partial\Omega \subset \mathbb{R}^d$, are permitted to move as the system of equations evolves in time. Knots are inserted, deleted, or rearranged in such a manner to conserve the extensive physical quantities of mass, momentum components, and total energy.

Our study consists of the following parts:

A. Local rotational and Galilean translational transformations can be obtained to reduce the conservation equations into steady state forms for the inviscid Euler equations or Navier-Stokes equations.

B. The entire set of PDEs are transformed into the method of lines approach yielding a set of coupled ordinary differential equations whose homogeneous solution is exact in time.

C. The spatial components are approximated by expansions of meshless RBFs; each individual RBF is volumetrically integrated at one of the sampling knots x_i, yielding a collocation formulation of the method of lines structure of the ODEs.

D. Because the volume integrated RBFs increase more rapidly away from the data center than the commonly used RBFs, we use a higher order preconditioner to counter-act the ill-conditioning problem. Domain decomposition is used over each piece-wise continuous subdomain.

*Embry-Riddle Aeronautical University, Oakland Center, 7700 Edgewater Dr., Oakland, CA 94621 USA, corresponding author

†The University of Nottingham, School of Mechanical, Materials, Manufacturing Engineering and Management, Nottingham, NG7 2 RD, United Kingdom

‡Department of Applied Mathematics, Illinois Institute of Technology, Chicago, IL 60616 USA

§Department of Mathematics, Simon Fraser University, Burnaby, B.C., Canada

1 Introduction

It has be shown that the order of convergence is reduced by the order of differentiation (see, e.g., Madych and Nelson's Theorem 4.4. in [30]). We therefore expect that a volumetric integral formulation of the time dependent conservation equations will increase the convergence rates of RBF approximates so even fewer knots will be required to discretize the problem domain. Although it is possible to generate a volumetric representation of RBFs for solid mechanics or other mechanics, this study will be limited to ideal gas-dynamics. Consider the strong form of the gas-dynamic conservation equations in compact form:

$$\frac{\partial \mathbf{U}}{\partial t} + \nabla \cdot \mathcal{F} = 0, \tag{1}$$

where the *flux* $\mathcal{F}$ is of the form

$$\mathcal{F}(\mathbf{U}) = \mathbf{F}_1(\mathbf{U})\mathbf{i} + \mathbf{F}_2(\mathbf{U})\mathbf{j} + \mathbf{F}_3(\mathbf{U})\mathbf{k}, \tag{2}$$

with $\mathbf{i}$, $\mathbf{j}$, and $\mathbf{k}$ representing the standard unit vectors along the Cartesian coordinate directions. In equation (1) the conserved quantities are the *mass density* ρ, the *momentum density components* $\mathbf{m} = m_1\mathbf{i} + m_2\mathbf{j} + m_3\mathbf{k}$, and the *energy density* E. They are collectively expressed as

$$\mathbf{U} = [\rho, m_1, E, m_2, m_3]^T.$$

All five components depend on time t and space $\mathbf{x} = x_1\mathbf{i}+x_2\mathbf{j}+x_3\mathbf{k}$. If we introduce the *flow velocity* $\mathbf{u} = u_1\mathbf{i} + u_2\mathbf{j} + u_3\mathbf{k}$, then the connection between momentum density and velocity is expressed as $\mathbf{m} = \rho\mathbf{u}$. Also, the *pressure* p is related to the total energy density E and the mass and momentum densities by the relation

$$p = (\gamma - 1)(E - \mathbf{m} \cdot \mathbf{m}/(2\rho)).$$

Here γ is the ratio of the specific heats at constant pressure to constant volume. The temperature T can be found from the pressure and the mass density by the ideal gas law

$$p = \rho R T,$$

where R is the universal gas constant. The *sound speed* a is given by the relation

$$a = \sqrt{\frac{\gamma p}{\rho}} = \sqrt{\gamma(\gamma - 1)\left[\frac{E}{\rho} - \frac{\mathbf{u} \cdot \mathbf{u}}{2}\right]}.$$

Using the notation introduced above, the fluxes in the directions of $\mathbf{i}$, $\mathbf{j}$ and $\mathbf{k}$ are

$$\begin{aligned} \mathbf{F}_1(\mathbf{U}) &= [m_1, m_1u_1 + p, (E + p)u_1, m_1u_2, m_1u_3]^T, \\ \mathbf{F}_2(\mathbf{U}) &= [m_2, m_2u_1, (E + p)u_2, m_2u_2 + p, m_2u_3]^T, \\ \mathbf{F}_3(\mathbf{U}) &= [m_3, m_3u_1, (E + p)u_3, m_3u_2, m_3u_3 + p,]^T. \end{aligned} \tag{3}$$

The conservation law (1) in three dimensions represents a system of five partial differential equations in the five unknowns of $\mathbf{U}$. In order to make this dependence explicit, we adopt the notation U_i, $i = 1, \ldots, 5$, for the components of $\mathbf{U}$ and $F_{k,i}$, $i = 1, \ldots, 5$, for the components of $\mathbf{F}_k$, $k = 1, 2, 3$. The fluxes are related to the array of conserved quantities by the Jacobian elements

$$A^k_{i,j} = \frac{\partial F_{k,i}}{\partial U_j}, \qquad i, j = 1, \ldots, 5, \quad k = 1, 2, 3.$$

An alternative way of writing the Euler conservation equations (1) for the i-th dependent variable is therefore

$$\frac{\partial U_i}{\partial t} + \sum_{k=1}^{3} \sum_{j=1}^{5} A^k_{i,j} \frac{\partial U_j}{\partial x_k} = 0.$$

The numerical solution of any system of coupled three-dimensional equations with standard finite difference, finite element, or finite volume codes is a large formidable undertaking. If the domain is irregular, the mesh generation may require weeks; the actual 3D calculations are typically limited to those organizations that have massively parallel machines.

Because hyperbolic PDEs in $\mathbb{R}^d$ can permit shocks that are in $\mathbb{R}^{d-1}$, we assume the dependent variables are piece-wise continuous in regions that are bounded by shocks, contact surfaces or material interfaces that form a continuous subdomain $\Omega \subset \mathbb{R}^{d-1}$. Over each Ω, the dependent variables, U_i, $i = 1, \ldots, 5$, are expanded in terms of piecewise continuous meshless radial basis functions (RBFs). The surfaces representing the shock or interfaces (points in 1D, curves in 2D, and surfaces in 3D) form the interface regions bounding the continuous subdomains. The philosophy used here is that whenever possible, we will track shocks and material interfaces. We will smear out shocks only in certain oblique collisions or when we wish to dampen small amplitude shocks that are not physically important by using shock-capturing methods requiring an artificial viscosity.

Because there is no knot connectivity involved, we have the freedom to permit knots to rotate and translate to convenient frames in which the physics are simpler. By abandoning meshes with connectivity restrictions on knots, we are free to use arbitrary Lagrangian methods, more general moving knot schemes, and permit rotations such as in the development of vortices without diffusive remappings periodically onto a fixed Eulerian frame. The only restriction that is placed upon knot motion is no knots can numerically coincide. After we have established that the physics represented by the transformed frames are simpler, we shall present the RBF approach, and numerical implementation issues such as preconditioners and domain decomposition.

1.1 Local Rotational Transformations

Deconinck, Hirsch, and Peutman [19] showed that the set of Euler equations could not be simultaneously "diagonalized" or transformed into a set of coupled one-dimensional PDEs by sets of simple rotations in the Eulerian frame. Recently, Kansa [26] showed that a subset of the multi-dimensional Euler equations could be cast into one-dimensional PDEs by a set of carefully chosen rotations for the mass, principal momentum, and total energy equations; the remaining stream-line bending momentum equations cannot be “diagonalized”. A summary of the derivation is presented here, and the reader is referred to Kansa [26] for the details of the derivation. The reason we cannot diagonalize all the conservation equations simultaneously is that the mass and total energy densities are scalar quantities that are invariant under rotation, whereas the momentum conservation equations are vector components that are not invariant under rotation.

In two dimensions, the coordinates that align with the components of the momentum are rotated about an angle θ so that the magnitude of the principal momentum is parallel to the x_1' axis. A single prime will be used to denote quantities after rotation. For the three dimensional case below we will use a second prime to denote quantities after the required second rotation.

In the rotated frame, the conservation of mass, principal momentum, and total energy density becomes

$$\begin{aligned}
\frac{\partial \rho}{\partial t} + \frac{\partial m_1'}{\partial x_1'} &= 0, \\
\frac{\partial m_1'}{\partial t} + \frac{\partial (m_1' u_1' + p)}{\partial x_1'} &= 0, \\
\frac{\partial E}{\partial t} + \frac{\partial \left((E+p)u_1'\right)}{\partial x_1'} &= 0,
\end{aligned}$$

where $u_1' = m_1'/\rho$. Note in this coordinate system, these conservation equations are one-dimensional. However, the remaining angular momentum equation is two-dimensional:

$$m_1' \left(\frac{\partial \theta}{\partial t} + u_1' \frac{\partial \theta}{\partial x_1'} \right) + \frac{\partial p}{\partial x_2'} = 0.$$

In three dimensions, two rotations are involved. The first rotation occurs in the $x_1 - x_2$ coordinate plane in which an angle θ is found that eliminates the component m_2' along x_2'. The second rotation through the angle ϑ is in the $x_1' - x_3$ system in which the momentum component m_3'' is zero along x_3'', leaving a non-zero component of momentum, m_1'', along x_1''. Here we specify that $x_2'' = x_2'$. The five conservation equations become

$$\begin{aligned}
\frac{\partial \rho}{\partial t} + \frac{\partial m_1''}{\partial x_1''} &= 0, \\
\frac{\partial m_1''}{\partial t} + \frac{\partial (m_1'' u_1'' + p)}{\partial x_1''} &= 0, \\
\frac{\partial E}{\partial t} + \frac{\partial \left((E+p)u_1''\right)}{\partial x_1''} &= 0, \qquad (4)
\end{aligned}$$

with the angular momenta equations that contribute to streamline bending being two-dimensional

$$\begin{aligned}
m_1' \left(\frac{\partial \theta}{\partial t} + u_1' \frac{\partial \theta}{\partial x_1'} \right) + \frac{\partial p}{\partial x_2'} &= 0, \\
m_1'' \left(\frac{\partial \vartheta}{\partial t} + u_1'' \frac{\partial \vartheta}{\partial x_2''} \right) + \frac{\partial p}{\partial x_3''} &= 0.
\end{aligned}$$

Here $u_1' = m_1'/\rho$ and $u_1'' = m_1''/\rho$.

The three-dimensional rotated PDEs are more complicated because two successive rotational transformations are required. Note that for the first rotation, we rotate m_1 and m_2 about the angle θ that forces m_2' to be zero along the coordinate x_2'. The second rotation about the x_2' axis rotates m_1' and m_3 so that $m_3'' = 0$ along x_3'', and the entire vector m_1'' is parallel to x_1''.

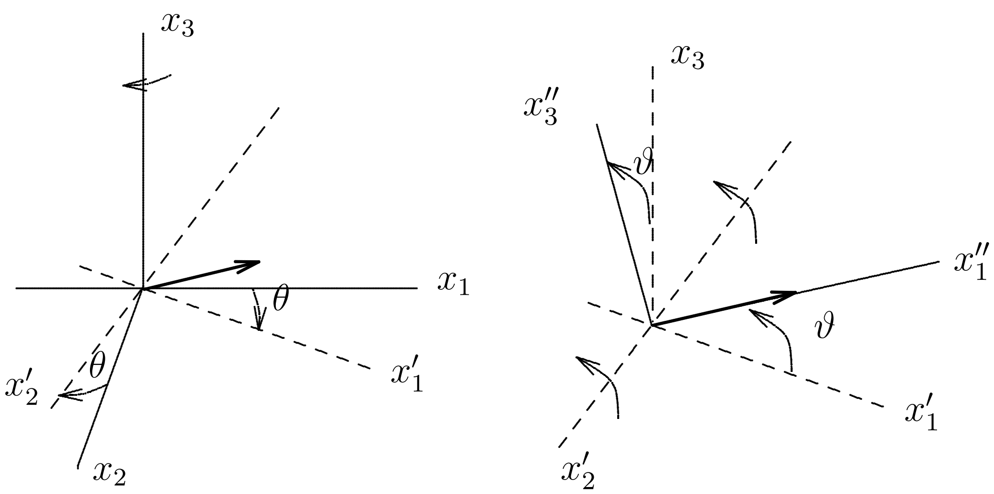

Figure 1: Rotation by θ eliminates $\rho\mathbf{v}$ component along x_2 axis. Rotation by ϑ eliminates $\rho\mathbf{w}$ component along x_3'' axis. Momentum $\rho u_1''$ is aligned with x_1'' axis.

1.2 Galilean Transformations for Ideal Gasdynamics

As we saw above, simple rotations can diagonalize at least three of the conservation equations. Next, we examine any benefits that may arise from Galilean translational transformations to the governing PDEs. Galilean transformations can be employed to cast the governing conservation equations into yet simpler equations by translating the local coordinate system by a suitable *frame velocity* $\mathbf{v}_i$ for the i-th dependent variable. Consider the conservation equations in the fixed Eulerian frame

$$\frac{\partial U_i}{\partial t} + \nabla \cdot \mathcal{F}_i = 0.$$

We can add and subtract a term, $\mathbf{v}_i \cdot \nabla U_i$, leaving the Eulerian frame conservation equation unchanged yielding

$$\frac{dU_i}{dt} + \nabla \cdot \mathcal{F}_i - \mathbf{v}_i \cdot \nabla U_i = 0,$$

where

$$\frac{dU_i}{dt} = \frac{\partial U_i}{\partial t} + \mathbf{v}_i \cdot \nabla U_i, \tag{5}$$

with dU_i/dt being the total derivative with respect to time in a translating coordinate system moving at the velocity $\mathbf{v}_i$. We shall denote the total derivative with respect to time of any variable as $\dot{} = \frac{d}{dt}$ to compress the notation.

Because diffusive processes transport flux, it is possible to define a diffusive velocity associated with diffusive flux transport, see Bird, Stewart, and Lightfoot [8]. With rotational and Galilean translational transformations, we have the freedom to choose the form of the set of coupled PDEs to be solved. Note that if viscous dissipation and thermal diffusion are present, shock waves are no longer discontinuities, but are spread out over a thin, finite region in the normal direction of propagation; material interfaces still remain discontinuous surfaces. Because rotations cannot reduce the dimensionality of the Navier-Stokes equations, two-dimensional and three-dimensional Navier-Stokes equations still retain their dimensionality. Thus, adding and subtracting $\mathbf{v}_i \cdot \nabla U_i$ to the Navier-Stokes equations yields

$$\frac{\partial U_i}{\partial t} + \mathbf{v}_i \cdot \nabla U_i + \nabla \cdot (\mathcal{F}_i + \mathcal{J}_i) - \mathbf{v}_i \cdot \nabla U_i = 0.$$

The diffusion flux for the momenta equations for $i = 2$, 4, and 5 is

$$\mathcal{J}_i = -\mu \nabla \mathbf{u}$$

and the diffusion flux for the total energy equation has contributions from both the viscous dissipation of momentum and thermal conduction that is given by

$$\mathcal{J}_3 = -\mathbf{u} \cdot (\mu \nabla \mathbf{u}) - \nabla \cdot (\mathbf{k} \nabla T)$$

where μ is the viscosity tensor, $\mathbf{k}$ is the thermal conductivity tensor, and T is the ideal gas temperature.

The *wavefront* $\dot{\mathbf{x}}_i$ is the wavepath along which $U_i = 0$. The following Galilean transformations presented here transform the spatial dependence away so steady equations need to be solved of the form

$$\dot{U}_i = \frac{\partial U_i}{\partial t} + \mathbf{v}_i \cdot \nabla U_i = 0 \quad \text{along} \quad \dot{\mathbf{x}}_i = \mathbf{v}_i.$$

Here $\mathbf{x}_i$, $i = 1, \ldots, 5$, denotes the knot location of component U_i (as opposed to x_k $k = 1, 2, 3$, that denotes the k-th coordinate of knot $\mathbf{x}$). Instead of $\mathbf{x}_{ik}$ we commonly denote the k-th coordinate of $\mathbf{x}_i$ by x_k hiding the dependence on i in the interest of more transparent notation. The knot velocity has components along each of the locally rotated coordinates because of the transformation.

By choosing the frame velocity $\mathbf{v}_i$ so that (5) is transformed to a steady equation, we have a much simpler system to solve. We choose $\mathbf{v}_i$ to be given by

$$\mathbf{v}_i = \begin{cases} \dfrac{\nabla \cdot (\mathcal{F}_i + \mathcal{J}_i)}{\nabla U_i \cdot \nabla U_i} \nabla U_i, & \text{if } |\nabla U_i| > 0, \\ \mathbf{0}, & \text{otherwise.} \end{cases} \tag{6}$$

Therefore

$$\dot{U}_i = 0 \quad \text{along} \quad \dot{\mathbf{x}}_i = \mathbf{v}_i.$$

Although it is not the intent to solve multi-dimensional Navier-Stokes equations in this paper, we presented a more general method to illustrate that this is possible. For the remainder of this paper, we shall assume that $\mathcal{J}_i = 0$, and that we are dealing with strictly hyperbolic problems.

Consider the conservation of mass, principal momentum, and total energy in the rotated frame that is translating at the velocity $\mathbf{v}_i$, where the unit vectors $\mathbf{e}_1$, $\mathbf{e}_2$, and $\mathbf{e}_3$, are along the rotated coordinates x_1'', x_2'', and x_3'', respectively. So

$$\mathbf{v}_i = v_{1,i}\mathbf{e}_1 + v_{2,i}\mathbf{e}_2 + v_{3,i}\mathbf{e}_3.$$

Since the conservation equations (4) are diagonalized, we can determine the components along x_1'' as

$$\begin{aligned}
\frac{\partial m_1''}{\partial x_1''} - v_{1,1}\frac{\partial \rho}{\partial x_1''} &= 0, \qquad v_{2,1} = v_{3,1} = 0,\\
\frac{\partial[m_1''u_1'' + p]}{\partial x_1''} - v_{1,2}\frac{\partial m_1''}{\partial x_1''} &= 0, \qquad v_{2,2} = v_{3,2} = 0,\\
\frac{\partial[(E+p)u_1'']}{\partial x_1''} - v_{1,3}\frac{\partial E}{\partial x''} &= 0, \qquad v_{2,3} = v_{3,3} = 0.
\end{aligned}$$

Since we want the x_1'' component of velocity, $\lambda_i = v_{1,i}$, to be simultaneously satisfied for all three equations, we find the eigenvalues of the Jacobian (see Toro [37], Chapter 3)

$$\det[\mathbf{J}] = \begin{vmatrix} -\lambda_i & 1 & 0 \\ \frac{(3-\gamma)u_1''^2}{2} & [(3-\gamma)u_1'' - \lambda_i] & 1 \\ \left[\frac{(\gamma-2)u_1''^3}{2} - \frac{a^2 u_1''}{(\gamma-1)}\right] & \left[\frac{a^2}{(\gamma-1)} + (3-2\gamma)u_1''^2\right] & [\gamma u_1'' - \lambda_i] \end{vmatrix} = 0.$$

The velocities for the mass, principal momentum, and total energy densities are linear combinations of the familiar characteristic velocities: $\lambda_1 = u_1'' - a$, $\lambda_2 = u_1''$, and $\lambda_3 = u_1'' + a$, where a is the sound speed. Associated with the characteristic velocities are three total time derivatives of the independent eigenvectors or compatibility variables denoted as $\dot{W}_i$ that are linear combinations of the total derivatives of mass, principal momentum, and total energy

$$\dot{W}_i = b_{i,1}\dot{\rho} + b_{i,2}\dot{m}_1'' + b_{i,3}\dot{E} = 0, \qquad i = 1,2,3. \tag{7}$$

Using the relations provided by Toro [37], the coefficients that depend upon the eigenvalue λ_i are

$$b_{i,3}(\lambda_i) = 1,$$

$$b_{i,2}(\lambda_i) = \frac{(\lambda_i - \gamma u_1'')}{(\gamma-1)},$$

$$b_{i,1}(\lambda_i) = \left(\frac{(\lambda_i - \gamma u_1'')}{(\gamma-1)}\right)\left(\lambda_i - (3-\gamma)u_1''\right) - \frac{a^2}{(\gamma-1)} - \frac{(2\gamma-3)u_1''^2}{2}.$$

The angular momenta density conservation equations are not one-dimensional but are two-dimensional. The first angular momentum compatibility equation is

$$\dot{W}_4 = m_1'\dot{\theta} = 0, \tag{8}$$

along

$$\dot{\mathbf{x}}_4 = \mathbf{v}_4 = \frac{\left[m_1'\frac{\partial\theta}{\partial x_1'} + \frac{\partial p}{\partial x_2'}\right]}{m_1'\left[(\frac{\partial\theta}{\partial x_1'})^2 + (\frac{\partial\theta}{\partial x_2'})^2\right]}\left(\frac{\partial\theta}{\partial x_1'}\mathbf{e}_1' + \frac{\partial\theta}{\partial x_2'}\mathbf{e}_2'\right).$$

The second angular momentum compatibility equation is

$$\dot{W}_5 = m_1''\dot{\vartheta} = 0 \tag{9}$$

along

$$\frac{d\mathbf{x}_5}{dt} = \mathbf{v}_5 = \frac{\left[m_1''\frac{\partial\vartheta}{\partial x_1''} + \frac{\partial p}{\partial x_3''}\right]}{m_1''\left[(\frac{\partial\theta}{\partial x_1''})^2 + (\frac{\partial\vartheta}{\partial x_3''})^2\right]}\left(\frac{\partial\vartheta}{\partial x_1''}\mathbf{e}_1'' + \frac{\partial\vartheta}{\partial x_3''}\mathbf{e}_2''\right).$$

According to (7), (8), (9) the coefficient matrix $\mathbf{Q}$ that transforms the total time derivatives of the dependent variables $\dot{U}$ into the total time derivatives of the compatibility (eigenvector) variables $\dot{W}$ is given by

$$\mathbf{Q}\dot{\mathbf{U}} = \begin{pmatrix} b_{1,1} & b_{1,2} & 1 & 0 & 0 \\ b_{2,1} & b_{2,2} & 1 & 0 & 0 \\ b_{3,1} & b_{3,2} & 1 & 0 & 0 \\ 0 & 0 & 0 & m_1' & 0 \\ 0 & 0 & 0 & 0 & m_1'' \end{pmatrix}\begin{pmatrix} \dot{\rho} \\ \dot{m}_1'' \\ \dot{E} \\ \dot{\theta} \\ \dot{\vartheta} \end{pmatrix} = \begin{pmatrix} \dot{W}_1 \\ \dot{W}_2 \\ \dot{W}_3 \\ \dot{W}_4 \\ \dot{W}_5 \end{pmatrix} = \dot{\mathbf{W}}. \tag{10}$$

The advantage of using the total time derivatives of the compatibility variables is that they are decoupled eigenvectors that are constant along the "characteristic velocities" $\dot{\mathbf{x}}_i$, $i = 1, \ldots, 5$. After we time advance the compatibility variables, we simply find the inverse transformation to find the time-advanced set of dependent variables.

At a time, t^n, we time advance the dependent variables from a common location, $\mathbf{x}_k$, onto five new locations at the advanced time. To avoid tracking a plethora of knots as the solutions advance in time, we offer the following recommendation. Let the knots move to the new positions, but afterwards, interpolate (remap) the set of dependent variables onto a common position at t^{n+1} given by $\dot{x}_i'' = u_{1,i}''$. This requires a very high order interpolation scheme to minimize the introduction of numerical diffusion that is common with low-order remapping schemes.

1.3 Shocks and Interfaces in the Rotated Galilean Frame

Idealized shocks, contact surfaces, and material interfaces are true discontinuous surfaces. Obtaining the velocities at discontinuities by derivative methods is an undefined process. At a shock, the characteristic velocities are degenerate. Mass, principal momentum and total energy are discontinuous at a shock, but the tangential velocity components are continuous. In addition, the streamlines are discontinuous across a shock. If the discontinuity is a material interface or contact surface, the interface moves with the principal fluid velocity. The pressure and normal fluid velocity are

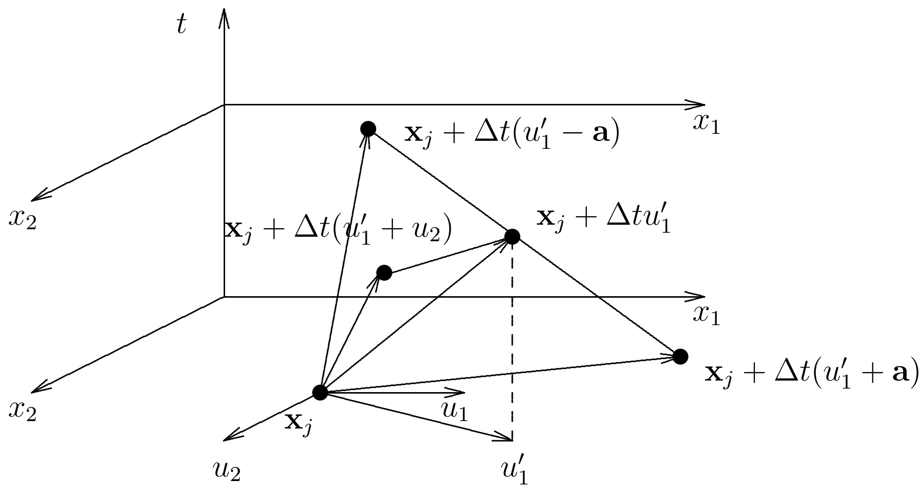

Figure 2: Knot locations before remap.

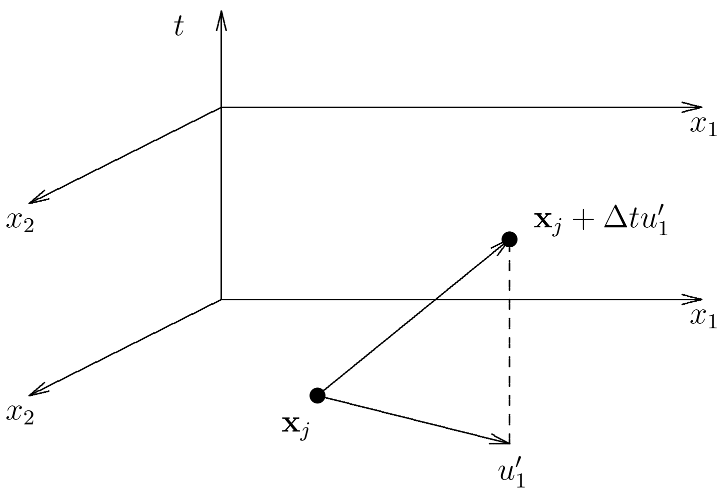

Figure 3: Common knot locations after remap.

continuous, but the mass density is discontinuous at a material interface. However, integration is a well-defined process across piece-wise continuous regions. Assume that we have rotated the dependent variables on either side of the discontinuity into the direction of the principal momentum. Let the superscripts $^+$ and $^-$ denote the dependent conservative form quantities on either side of the discontinuity. Notice the streamline bends across the shock and the angles θ^- and θ^+ are different, but the tangential velocity components, $u_2^- = u_2^+$ as are the tangential pressure gradients along the shock.

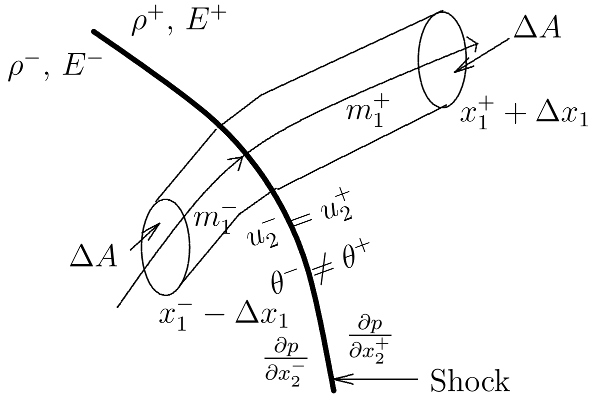

Figure 4: Setup for integration across a shock discontinuity to determine the Rankine-Hugoniot relations.

Consider a volume element $dV = \Delta A dx_1''$ where ΔA is the area segment along the principal momentum m_1'' that is parallel to the rotated coordinate x_1'' on either side of the discontinuity. The integral of the fluxes across the discontinuity gives (after dropping ΔA)

$$\int_{(x_1'')^-}^{(x_1'')^+} \left(\frac{\partial \mathcal{F}_i}{\partial x_1''} - \mathbf{v}_i \frac{\partial U_i}{\partial x_1''} \right) dx_1'' \Delta A = 0,$$

that in the general case leads to

$$\left(\mathcal{F}_i^+ - \mathcal{F}_i^- \right) - v_{1,i} \left(U_i^+ - U_i^- \right) = 0.$$

Solving for $v_{1,i}$ gives the familiar Rankine-Hugoniot relations

$$v_{1,1} = \frac{(m_1'')^+ - (m_1'')^-}{\rho^+ - \rho^-}, \qquad v_{2,1} = v_{3,1} = 0,$$
$$v_{1,2} = \frac{[m_1'' u_1'' + p]^+ - [m_1'' u_1'' + p]^-}{(m_1'')^+ - (m_1'')^-}, \qquad v_{2,2} = v_{3,2} = 0,$$
$$v_{1,3} = \frac{[(E+p)u_1'']^+ - [(E+p)u_1'']^-}{E^+ - E^-}, \qquad v_{2,3} = v_{3,3} = 0.$$

Along two points, **a** and **b**, that lie tangent along the interface surface, we have the following jump conditions across the shock:

$$
\begin{aligned}
v'_{1,4} &= \frac{[(m'_1 u'_1 + p)\theta]^+ - [(m'_1 u'_1 + p)\theta]^-}{[m'_1\theta]^+ - [m'_1\theta]^-}, \\
v'_{2,4} &= \frac{[p^{\mathbf{b}} - p^{\mathbf{a}}]^+ - [p^{\mathbf{b}} - p^{\mathbf{a}}]^-}{(m'_1)^+[\theta^{\mathbf{b}} - \theta^{\mathbf{a}}]^+ - (m'_1)^-[\theta^{\mathbf{b}} - \theta^{\mathbf{a}}]^-}, \\
v''_{1,5} &= \frac{[(m''_1 u''_1 + p)\vartheta]^+ - [(m''_1 u''_1 + p)\vartheta]^-}{[m''_1\vartheta]^+ - [m''_1\vartheta]^-}, \\
v''_{3,5} &= \frac{[p^{\mathbf{b}} - p^{\mathbf{a}}]^+ - [p^{\mathbf{b}} - p^{\mathbf{a}}]^-}{(m''_1)^+[\vartheta^{\mathbf{b}} - \vartheta^{\mathbf{a}}]^+ - (m''_1)^-[\vartheta^{\mathbf{b}} - \vartheta^{\mathbf{a}}]^-}.
\end{aligned}
$$

Shock capturing has been the preferred manner in modeling, especially with mesh-based Eulerian or Lagrangian methods. Shock tracking has been used as an alternative approach because the shock is treated as a discontinuity ([17] and [24]). Shock capturing has long been the preferred manner to detect developing shocks, but this approach can also be done in a moving knot scheme and monitoring the characteristic velocities as they develop in time.

Remark 1. By transforming the local coordinate system by rotations and Galilean transformations, we change the complicated inviscid Euler and Navier-Stokes equations into simple forms that may even have exact time dependent solutions. However, the price one pays for this simplification is a rotated moving set of knots for each compatibility variable W_i. We will require very accurate interpolation or spatial partial derivative estimates to implement this approach.

Remark 2. The set of velocities $\mathbf{v}_i$ are proportional to the combined advective and diffusive flux gradients in the stream-wise direction; the larger these gradients become, the faster are such Galilean velocities. The knots are free to move, but must not be allowed to coincide numerically because the resulting system of equations would be singular. Several strategies can be employed. If there is a locus of knots tending to coincide, such as the formation of a shock, we can extrapolate forward in time and replace those coincident knots with a discontinuous surface. Whenever knots are redistributed, added or deleted, the dependent variables need to be interpolated onto the new distribution of knots, but in a strictly conservative manner.

Remark 3. One-dimensional shock collisions with other shocks, boundaries, contact surfaces, or material interfaces are best modeled with Riemann solvers (see Toro [37]) by rotating into the direction of principal momentum. The resultant outgoing waves can be various combinations of rarefaction fans and shocks with a contact surface in between such waves. Multidimensional shock collisions with Riemann solvers (see Toro [37]) are sometimes treated by splitting along the rotated coordinate axes. Shocks and contact surfaces are true discontinuities. A rarefaction fan is a continuous region that is bounded by either left or right fan of characteristics in which the entropy is constant in that region. A rarefaction fan is continuously varying, and the dependent variables are continuous at the endpoints of the fan. However, the normal gradients from the left and the right at the endpoints of the rarefaction fan are not necessarily equal. For this reason, one should track the characteristics from the rarefaction fans to prevent any artificial numerical requirements that the function and its normal gradient at the endpoints be the same from the left and the right.

2 Boundary Conditions

The proper specification of boundary conditions is essential to the well posedness of hyperbolic partial differential equations. Basic to the application of boundary conditions is the realization that the governing PDEs apply everywhere on the domain Ω and have specific forms on the boundary $\partial\Omega$. The reason for recasting the boundary constraints is a mathematical convenience that permits us to transform the PDEs into systems of ordinary differential equations (ODEs) over the entire domain; this will be discussed later. It is convenient to consider the generalized compatibility dependent variables W_i, $i = 1, \ldots, 5$, that exist along the conventional characteristic velocities $\mathbf{v}_i$.

The literature has dealt with two general classes of boundary conditions as (see Laney [28])

- in-flow and out-flow boundary conditions,
- algebraic constraints.

Note, at the initial time, all the dependent variables are specified over the entire domain. This initial value problem can be considered equivalent to an interpolation problem.

2.1 In-flow and Out-flow Boundary Conditions

In-flow and out-flow boundary conditions in the rotated frame can be conveniently understood in terms of the characteristic velocities. A compatibility equation is applicable at an inflow or outflow velocity if its characteristic, $\dot{\mathbf{x}}_i = \mathbf{v}_i$, lies within the domain Ω. Otherwise, it is not applicable.

Laney [28] showed that the number of possible inflow boundary conditions depends on whether the flow velocity $(u > 0)$ is supersonic or subsonic. If the one-dimensional flow is supersonic, then three dependent variables need to be specified. But if the inflow velocity is subsubsonic, then two dependent variables need to be specified. Laney [28] showed that at the out-flow boundary with $(u > 0)$ one dependent variable must be specified if the flow is subsonic, and no dependent variables are to be specified if the flow is supersonic.

There is considerable debate regarding the treatment of far-field boundary conditions. At the surface denoted by S_∞, this boundary should be non-reflecting, and only transmitting. In reality, S_∞ propagates outward in time. Rather than fixing the position of the far-field boundary for all time at some large distance from the interesting action, we will permit this far-field boundary to propagate in time. This will avoid the problem of a wave with any appreciable magnitude interacting with the far-field boundary.

2.2 Algebraic Constraint Boundary Conditions

For hyperbolic equations, care must be used to avoid over-specifying boundary conditions. The so-called reflective boundary conditions can easily be considered as a special case of algebraic constraints.

Assume that subsonic inflow velocity is specified at some $\mathbf{x}_{B,i}$ that is fixed, for example, at the plane $x = 0$ for all time, then the inflow velocity is an auxiliary constraint that is constant for all time. However, the value of mass and total energy density is found by the solution of the compatibility equation along the incoming characteristic. This gives (see (7))

$$\dot{W}_1 = b_{1,1}\dot{\rho} + b_{1,2}\dot{m}_1'' + \dot{E} = 0$$

along the characteristic $u_1'' - c = 0$. The compatibility equation is solved simultaneously with the auxiliary constraint

$$\dot{u}_1'' = \frac{\dot{m}_1'' - u_1''\dot{\rho}}{\rho} = 0.$$

Similarly, if a boundary is a rigid wall, the gas velocity is always zero, and $\dot{u}_1'' = 0$. A similar procedure can be applied.

In another example, we may have a Dirichlet condition in which the inflow pressure is prescribed to be constant. Along an appropriate characteristic, $\dot{x}_1'' = \lambda_i$, we solve the compatibility equation

$$\dot{W}_i = b_{i,1}\dot{\rho} + b_{i,2}\dot{m}_1'' + \dot{E} = 0$$

simultaneously with the auxiliary constraint $\dot{p} = 0$.

In two or three dimensions, we may have Neumann normal gradients specified at boundaries, such as at symmetry boundaries. Suppose we have a situation in which we specify that $\frac{\partial p}{\partial x_2'} = 0$. The appropriate PDE and the auxiliary constraint are

$$m_1'\dot{\theta} + m_1'[u_1' - v_{4,1}]\left(\frac{\partial \theta}{\partial x_1'}\right) + \left(\frac{\partial p}{\partial x_2'} - v_{4,2}m_1'\frac{\partial \theta}{\partial x_2'}\right) = 0,$$
$$\frac{\partial p}{\partial x_2'} = 0.$$

The specification of the auxiliary condition $\frac{\partial p}{\partial x_2'} = 0$ implies that $v_{4,2} = 0$, but $v_{4,1} = u_1'$, and we have

$$m_1'\dot{\theta} = 0 \quad \text{along} \quad \dot{x}_1' = u_1'.$$

With these examples, we illustrated that either Dirichlet or Neumann boundary conditions can be implemented by combining the compatability equations along the appropriate "characteristic" velocities with the appropriate auxiliary constraints. The motivation for casting the boundary conditions in this manner will be clarified later.

If we consider a problem that has shocks and material interfaces that separate subdomains, these discontinuities propagate in time at a velocity determined by the Rankine-Hugoniot jump conditions. So the "boundaries" of a problem can have a fixed location or can propagate.

3 Radial Basis Function Formulation

Realizing that the PDEs apply at the boundary together with appropriate auxiliary constraints, we select those rotational and translational transformations on the multi-dimensional set of coupled PDEs converting them into coupled ODEs. By further transforming the dependent variable ODEs into the compatibility ODEs, we now have a set of independent ODEs in terms of the compatibility variables. Because the knots are permitted to move as dictated by the physics, we need to choose a convenient spatial representation. Our intent is to formulate the numerical solution of the physical problem in such a manner so as to reduce the PDE problem into a set of uncoupled ODE problems that are solved by the method of lines.

For the numerical solution of PDEs, the question is the manner in which a finite set of knots, $\mathbf{x} \in \mathbb{R}^d$, be used to represent either a continuous or piece-wise continuous set of functions. The standard approaches are to discretize the domain by meshes, and assume that a low order multi-dimensional Lagrangian polynomial in a mesh cell captures the spatial behavior of the dependent variables. It is commonly perceived that a compactly supported representation gives a well-conditioned set of linear equations. However, because the number of equations grows very large because of low order convergence rates, this perceived advantage is not necessarily true.

By differentiating this low order polynomial, one obtains difference schemes or derivatives in the mesh. One noticeable problem is that such polynomials are not splines, and the derivatives at the mesh boundaries can be discontinuous, although some complex schemes have been devised to ensure derivative continuity. Furthermore, low order polynomials are preferred because of the notorious polynomial "snaking" problem that causes derivative estimates to be very poor. Some higher order compact differencing schemes have been used with limited success. Finite volume methods are preferred because anti-differentiation or integration is more numerically stable, but again, the low order polynomial integration still requires very fine meshing in spatial regions where the dependent variables change dramatically. Theoretically, in the limit of the mesh spacing, $h \rightarrow 0$, the numerical solution transitions smoothly onto a piece-wise continuous function; in practice, no computer has an infinite memory or calculates infinitely fast.

The generation of a mesh, especially over irregular domains in three dimensions, can be a very tedious task. We therefore prefer the use of meshfree radial basis functions. Franke [23] evaluated over thirty scattered data interpolation methods against the performance of six analytic two-dimensional test functions. He ranked various scattered data interpolants such as the inverse distance method, the modified Shepard's function, and triangular and quadrilateral finite elements, etc. very poorly. Franke [23] concluded that the multiquadric (MQ) and thin-plate spline (TPS) radial basis functions (RBFs) performed optimally on all test functions and scattered data sets. With some powerful scattered data interpolants, it is easy to apply RBFs to the numerical solutions of PDEs and to use RBFs in the context of the boundary element method. Madych and Nelson [30] showed that the MQ and TPS RBFs enjoy exponential convergence. Chui et al. [18] showed that RBFs are wavelets with dilatational, rotational and translational properties and are very good for detecting discontinuities.

A univariate function ϕ becomes a *radial basic function* in a space $\mathbb{R}^d$ of dimension

d by composition with the Euclidean norm, i.e., a radial basic function is of the form $\varphi(\mathbf{x}) = \phi(\|\mathbf{x}\|)$. A basis for an appropriate finite-dimensional approximation space is then generated by selecting a set of *centers* $\mathbf{x}_j$, $j = 1, \ldots, N$, and centering ϕ at these points, i.e., the approximation space is given by $\text{span}\{\phi(\|\mathbf{x} - \mathbf{x}_1\|), \ldots, \phi(\|\mathbf{x} - \mathbf{x}_N\|)\}$.

There are an infinite number of possible univariate RBFs. If we let r be the Euclidean distance between any pair of points in the domain Ω, then some of the more commonly employed RBFs are:

- piecewise smooth splines

$$\begin{array}{ll} \phi(r) = -r^{2j+1} & \text{power spline,} \quad j \geq 0, \\ \phi(r) = r^2 \log(r) & \text{thin-plate spline,} \\ \phi(r) = (1-r)_+^m p(r) & \text{(CS-RBF) spline,} \end{array}$$

  where $p(r)$ is a polynomial of the Wendland (1995) compactly supported (CS-RBF) spline,

- infinitely smooth splines

$$\begin{array}{ll} \phi(r) = -\sqrt[\beta]{r^2 + c^2}, & \text{general multiquadric spline,} \\ \phi(r) = e^{-cr}, & \text{exponential spline,} \\ \phi(r) = e^{-cr^2}, & \text{Gaussian spline,} \\ \phi(r) = e^{-cr} K_\nu(cr), & \text{Matern spline,} \end{array}$$

  with K_ν a modified Bessel function of order ν.

Wen Chen [13],wch02a,wch02b,wch02c has pointed out that many of the RBFs are related to the solutions of PDEs. For example, it is well-known that the MQ-RBF is a solution to the biharmonic PDE. The optimal choice of an RBF to be used in various possible PDE problems is an ongoing research effort.

However, despite of the very nice convergence properties, meshless RBF methods have not been applied at present to large-scale PDE simulations. One of the main reasons is that both the global and compactly supported RBFs give rise to either very large full matrices, or large wide-banded matrices that are known to be very ill conditioned. The best convergence with CS-RBFs occurs as the support become increasingly more global unless a multilevel scheme is invoked. As explained by Schaback [34], the demand for high accuracy has associated with it a very ill conditioned system of equations. This observation is true if the system of equations were to be solved only by direct methods such as Gaussian elimination with pivoting.

However, domain decomposition and suitable preconditioners combined with fast multipole expansions permit very efficient fast iterative methods without the need to store matrix elements. The recent development in domain decomposition and preconditioners makes the use of meshless RBFs in the solution of PDEs very attractive. These topics will be addressed later.

We shall discuss two methods of obtaining the advanced time solutions based upon the transformations introduced to solve the compatibility ordinary differential equations (ODEs). The first method uses the collocation method in which the Galilean velocities are determined by gradient methods, and the second method volume integrates the spatial portion of the compatibility equations and determines the Galilean velocities by application of Gauss's theorem to the integral velocities. Although many of the operations in either approach are similar, there are some differences that will be summarized.

4 Recasting the Conservation PDEs in terms of RBFs using an Unsymmetric Collocation Approach

In order to simplify the notation, we will drop as many subscripts and superscripts as possible now. Even though we may deal with many dependent variables, compatibility variables, and physical subdomains simultaneously, we will only discuss a typical compatibility variable, domain and boundary surface for simplicity.

The preliminary starting point of the use of RBFs to solve PDEs is the interpolation problem that is equivalent to solving the initial value problem. At the initial time, let us assume a hyperbolic problem in which there exists either a material interface, a "moderate to strong" shock, or contact surface. We do not treat this initial problem as a global problem, but as a union of problems over piecewise smooth subdomains, and track discontinuities. It shall be understood that in the presentation of the collocation and the integral formulation we are dealing with the problem over the subdomain, Ω, in which the space and time are separable and the dependent variables are piece-wise continuous.

The initial condition (and subsequent solution) of the initial value problem is approximated as a linear combination of radial basis functions $\phi(\|\cdot - \mathbf{x}_j\|)$ and polynomials p_l of degree $l < K$ with a corresponding set of time dependent expansion coefficients $\alpha_j(t)$, i.e.

$$U(\mathbf{x}, t) = \sum_{j=1}^{N} \phi(\|\mathbf{x} - \mathbf{x}_j\|)\alpha_j(t) + \sum_{l=0}^{K-1} p_l(\mathbf{x})\beta_l(t).$$

In order to ensure a unique solution of the resulting system of linear equations we add the constraints

$$\sum_{j=1}^{N} \alpha_j(t) p_l(\mathbf{x}_j) = 0, \qquad \text{for } l = 0, 1, 2, \ldots, K-1.$$

Given a set of initial values of a variable U specified at N distinct knots, $\mathbf{U} = \{U_1, U_2, \ldots, U_N, 0, 0, \ldots, 0\}$, where $U_i = U(\mathbf{x}_i, t = 0)$, the vector of expansion coefficients $\sigma = [\alpha, \beta]^T$ is a solution to the following set of linear equations of the form $\mathbf{A}\sigma = \mathbf{U}$ where the matrix is given by

$$\mathbf{A} = \begin{pmatrix} \mathbf{\Phi} & \mathbf{P} \\ \mathbf{P^T} & \mathbf{0} \end{pmatrix}, \tag{11}$$

with

$$
\mathbf{\Phi} = \begin{pmatrix} \phi_{1,1} & \cdots & \phi_{1,N} \\ \vdots & & \vdots \\ \phi_{N,1} & \cdots & \phi_{N,N} \end{pmatrix},
$$

$\phi_{i,j} = \phi(\|\mathbf{x}_i - \mathbf{x}_j\|)$, $i, j = 1, \ldots, N$, and

$$
\mathbf{P} = \begin{pmatrix} p_0(\mathbf{x}_1) & \cdots & p_{K-1}(\mathbf{x}_1) \\ \vdots & & \vdots \\ p_0(\mathbf{x}_N) & \cdots & p_{K-1}(\mathbf{x}_N) \end{pmatrix}.
$$

Now we generalize the notation slightly and let Ψ be the generalized set of basis functions,

$$
\mathbf{\Psi} = \{\psi_1, \ldots, \psi_N, \psi_{N+1}, \ldots, \psi_{N+K}\} = \{\phi(\| \cdot - \mathbf{x}_1\|), \ldots, \phi(\| \cdot - \mathbf{x}_N\|), p_0, \ldots, p_{K-1}\}.
$$

Also, let the generalized expansion coefficients σ be given by

$$
\sigma = [\alpha_1, \alpha_2, \ldots, \alpha_N, \beta_0, \beta_1, \ldots, \beta_{K-1}]^T.
$$

The initial value problem can be restated as the solution of the interpolation problem compactly as

$$
\mathbf{A}\sigma = \mathbf{U},
$$

where

$$
\mathbf{A} = \left(\begin{array}{ccc|ccc} \psi_{1,1} & \ldots & \psi_{1,N} & \psi_{1,N+1} & \cdots & \psi_{1,N+K} \\ \vdots & \ddots & \vdots & \ddots & \vdots & \\ \psi_{N,1} & \ldots & \psi_{N,N} & \psi_{N,N+1} & \cdots & \psi_{N,N+K} \\ \hline \psi_{N+1,1} & \ldots & \psi_{N+1,N} & \mathbf{0} & \ldots & \mathbf{0} \\ \vdots & \ddots & \vdots & \ddots & \vdots & \\ \psi_{N+K,1} & \ldots & \psi_{N+K,N} & \mathbf{0} & \ldots & \mathbf{0} \end{array}\right).
$$

The expansion coefficients for each dependent variable are given by

$$
\sigma = \mathbf{A}^{-1}\mathbf{U}.
$$

The matrix $\mathbf{A}$ has the identical form to the interpolation matrix (11) and is theoretically invertible.

Given the initial conditions and the initial volume, we calculate the extensive quantities of mass, momentum components, and total energy on each physical sub-domain. The sum of these quantities over the entire domain must be constant, since we have no source terms in the original Euler equations.

In order to time advance the solution from the initial values, we require some intermediate steps.

1. Construct the flux vector components at the current time from the dependent variables, using (3). Next, find the expansion coefficients for each one of the flux vector components using the existing inverse.

2. Find the local set of rotation angles. By using (6), find the set of moving knot velocities for each dependent variable.

3. Transform the set of expansion coefficients corresponding to each dependent variable U_k into the set of expansion coefficients for the independent compatibility variables, by using (10).

4. For notational compactness, define another set of basis functions

$$\chi = \mathbf{v} \cdot \nabla \psi$$

that depends upon the different characteristic velocities.

There is a matrix $\mathbf{B}$ that pre-multiplies the set of expansion coefficients $\sigma(\mathbf{t})$ that is given by

$$\mathbf{B} = \left(\begin{array}{ccc|ccc} \chi_{1,1} & \cdots & \chi_{1,N} & \chi_{1,N+1} & \cdots & \chi_{1,N+K} \\ \vdots & \ddots & \vdots & \ddots & \vdots & \\ \chi_{N,1} & \cdots & \chi_{N,N} & \chi_{N,N+1} & \cdots & \chi_{N,N+K} \\ \hline \chi_{N+1,1} & \cdots & \chi_{N+1,N} & \mathbf{0} & \cdots & \mathbf{0} \\ \vdots & \ddots & \vdots & \ddots & \vdots & \\ \chi_{N+K,1} & \cdots & \chi_{N+K,N} & \mathbf{0} & \cdots & \mathbf{0} \end{array} \right).$$

The matrix $\mathbf{B}$ will contain the information of the boundary auxiliary constraints along the appropriate characteristic velocity $\mathbf{v}_i$.

5. We cast the compatibility equations into the method of lines formulation in which there is a system of $N + K$ equations in $N + K$ unknowns that is compactly represented as

$$\mathbf{A}\frac{d\sigma}{dt} + \mathbf{B}\sigma = 0. \tag{12}$$

6. This set of ODEs has a solution that is given by

$$\sigma(t^{n+1}) = \exp(-\mathbf{R})\sigma(t^n) = \left(\mathbf{I} + \sum_j \frac{(-\mathbf{R})^j}{j!} \right) \sigma(t^n), \tag{13}$$

where $\mathbf{R} = -\mathbf{A}^{-1}\mathbf{B}\Delta t$.

The homogeneous part of the differential equation has a matrix exponential time dependency that can be expanded in a Taylor series. We present this approach because the Crank-Nicholson method is only second order accurate in time. Depending upon the norm of the matrix $\mathbf{R}$ we can simply add more product terms until the truncation error is sufficiently small.

Because each compatibility variable has associated with it a different characteristic velocity vector, each compatibility variable will be located at a different knot. Before another time advance is made, we will interpolate the compatibility variables onto a common location specified by

$$x''_j(t^{n+1}) = x''_j(t^n) + \Delta t u''_{1,j}.$$

Then we apply the inverse rotations to obtain the location in the new Eulerian frame. After the expansion set $\sigma(t^{n+1})$ has been found for each W_i, we can easily recover the corresponding expansion coefficients for the strong conservative form dependent variables U_k by taking the inverse of equation (10).

5 RBF Volumetric Formulation

Madych and Nelson [30] have shown in their Theorem 4.4 that successively higher derivatives of the interpolant have their convergence rates reduced by the order of differentiation. It is well known that integration is always a smoothing operation. Our intent is to use anti-differentiation upon the divergences of fluxes and gradients of dependent variables to

1. obtain better estimates of the moving knot velocities to construct the characteristic velocities,
2. ensure the physics is being properly simulated by guaranteeing strict conservation of mass, momentum components, and total energy, and
3. converge faster than the knot collocation method.

Mai-Duy and Tran-Cong [31], [32] obtained very impressive computational results with singly or doubly integrated MQ RBFs that they cast as a minimization of the least-squares residual errors to find the expansion coefficients. Our approach uses the volume integrated RBFs over each piecewise continuous subdomain with a corresponding boundary surface. Our integration approach is physically meaningful since only the extensive volume integration of the various density functions obey strict conservation laws. Thus, we now deal with the integral form of the PDEs, i.e., the conservation law (1) is viewed as

$$\int_\Omega \left[\frac{\partial \mathbf{U}}{\partial t} + \nabla \cdot \mathcal{F}\right] dV = 0.$$

The union of the physical subdomains that are bounded by the physical boundaries and discontinuous surfaces is the model domain $\bigcup_\zeta \Omega_\zeta = \Omega$. Hence the sum of the volumes associated with each subdomain is the total volume of the domain. The set intersection of different subdomains is the set of discontinuous surfaces between the subdomains.

We modify the basis functions to be integrals of the RBFs evaluated at the discrete knots. This still gives the method of lines approach that forms an ODE system over all expansion coefficients, but we treat interior and boundary integrated RBFs differently. Thus, this procedure still yields coefficient matrices that pre-multiply the column vectors $\frac{d\sigma}{dt}$ and σ.

The procedures are somewhat similar to the collocation formulation. However, there are some notable exceptions such as the interpolation coefficient matrix $\mathbf{A}$ is replaced by one in which the elements are definite volume integrals. The elements of the coefficient matrix $\mathbf{B}$ are definite volume integrals of $\mathbf{v} \cdot \Psi$ in which Gauss's theorem is applied.

Step 1. Initialize the expansion coefficients at time $t = 0$.

Step 2. Construct the flux vector expansion coefficients.

Step 3. Determine the local rotation angles; then determine the Galilean translation velocities by using the integrated version of (6).

Step 4. Construct the RBF integral matrices.

Step 5. Time-advance the set of expansion coefficients for each compatibility variable.

Step 6. Interpolate knots associated with each dependent compatibility variable to a common location in a strictly conservative manner.

Step 7. Recover the conservation dependent variables.

Step 8. Determine new states from shock wave collisions if needed.

Step 9. Insert new discontinuous surface if required.

Step 10. Return to Step 2 until the calculation has reached the final time.

5.1 Implementation of Surface and Volume Integration

In this situation, we replace the previous matrices, $\mathbf{A}$ and $\mathbf{B}$ by the counterpart of the integrated basis functions to form new matrices. The objective is to calculate the RBF integrals over irregularly shaped subdomains Ω in the simplest manner possible. We require integration limits that would be simple lines or analytic curves in 2D or simple planar or analytic curved surfaces. The accepted procedure is to construct a mesh with Voronoi and Delaunay tessellation. The knots move in time and a new integration mesh needs to be computed every time step with a computational overhead. This tessellation method is certainly one possible procedure.

What we present here can be readily performed on parallel computers. We can partition the domain into convenient rectangles and/or triangles for a 2D domain, or bricks and/or pyramids in 3D whose volume element is denoted by dV_i, so that for each knot $\mathbf{x}_i$ we have a corresponding subdomain Ω_i. We permit these volume elements to overlap. The integration over each volume element over the basis functions $\psi(\cdot - \mathbf{x}_j)$ and $\chi(\cdot - \mathbf{x}_j)$ can be performed analytically or numerically in parallel mode, and the overlap contributions then subtracted in a pairwise fashion. Chen [11, 12] considered a moving least squares procedure for performing such integrations.

For illustration purposes, consider a 2D domain over a unit square, whose knots are labeled as $(0, 0)$, $(0, 1)$, $(1, 1)$, and $(0, 1)$. It is convenient to represent such knots in terms of (x, y) pairs. The row corresponding to the interior knot $\mathbf{x}_i = (x_i, y_i)$ is given by

$$\mathbf{A}_{i,j} = \int_{\Omega_i} \psi(\mathbf{x} - \mathbf{x}_j)\ dV_i - \text{overlap}.$$

We conjecture that as long as each interior knot $\mathbf{x}_i$ is computationally distinct, the rows of the matrix will be distinct. Similarly, we form the matrix $\mathbf{B}$ using the basis functions χ using the Gauss divergence theorem.

Integrating the d-dimensional RBFs over a surface of dimension $d-1$ forms the surface boundary integrals, and consequently the appropriate rows of the coefficient matrices. These integrals are evaluated along a closed contour. For example, consider a unit square. The integration has four steps.

A. Here we have a constant $x = 0$, and integrate from $y = 0$ to $y = 1$,

B. Here we have a constant $y = 1$, and integrate from $x = 0$ to $x = 1$,

C. Here we have a constant $x = 1$, and integrate from $y = 1$ to $y = 0$,

D. Here we have a constant $y = 0$, and integrate from $x = 1$ to $x = 0$.

In this example, we use two-dimensional RBFs, but integrate either along a constant x or a constant y. The first M rows forming the matrix elements are linearly independent, and the columns range over all the knots over the domain.

5.2 Time-advancing the Set of Expansion Coefficients

Note that the above matrices $\mathbf{A}$ and $\mathbf{B}$ yield a set of $N+K$ ODEs in $N+K$ expansion coefficients like (12). Similar to the knot collocation procedure, the advanced time expansion coefficients for the compatibilty variables are given by (13). We find the set of time-advanced coefficients corresponding to each compatibility variable W_i.

5.3 Interpolating Knots Associated with each Compatibility Variable to a Common Location

For each compatibility variable W_i the position of the j-th knot in Ω has been advanced to a location given by

$$\mathbf{x}_j^{n+1} = \mathbf{x}_j^n + \mathbf{v}_j \Delta t.$$

We want to interpolate onto a common location that is based upon the advection of the knot to this principal flow velocity given by

$$\mathbf{x}_j^{n+1} = \mathbf{x}_j^n + u''_{1,j} \Delta t.$$

We already have the information to perform this operation in a strictly conservative manner. The matrix $\mathbf{A}$ does not change for different characteristic velocities, whereas the matrix $\mathbf{B}$ does. Denote the matrix corresponding to the characteristic velocity u''_1 as $\mathbf{B}_0$. Define $\mathbf{R}_0 = \mathbf{A}^{-1}\mathbf{B}_0$ for convenience.

The extensive compatibility variable at the new time is

$$\mathcal{W}_i(t^{n+1}) \quad = \quad (\mathbf{A} + \Delta t \mathbf{B}_0)\, \sigma_i(t^{n+1})$$

$$= \mathbf{A}\sigma_i(t^n) - (\Delta t)^2(\mathbf{B}_0\mathbf{R}_0)\left(\frac{1}{2} - \frac{\Delta t\mathbf{R}_0}{3} + \frac{3(\Delta t\mathbf{R}_0)^2}{8} + \cdots\right)\sigma_i(t^n).$$

Dropping higher order terms in Δt has the interpretation that the compatibility variable at the new time is due to the advective transport along the principal flow velocity. All the extensive compatibility variables are remapped onto this common location. To find the extensive dependent variables at the new common location, we simply apply the inverse transform (10).

5.4 Treatment of Solutions at Propagating Interfaces

Although we have introduced some ideas about propagating shocks, contact surfaces, material interfaces and rarefaction fans, we need to discuss the implementation of this important area of physics in more detail. It is important to realize that our goal is to model the physics contained in the PDEs and boundary conditions correctly.

The nonlinear hyperbolic PDEs permit the formation of new shocks from previously continuous subdomains. This formation does not occur instantaneously, but is characterized by the tendency of knots to coincide onto a "surface". Shock capturing is not necessary using a uniform fine set of discretized knots to detect the formation of new shocks.

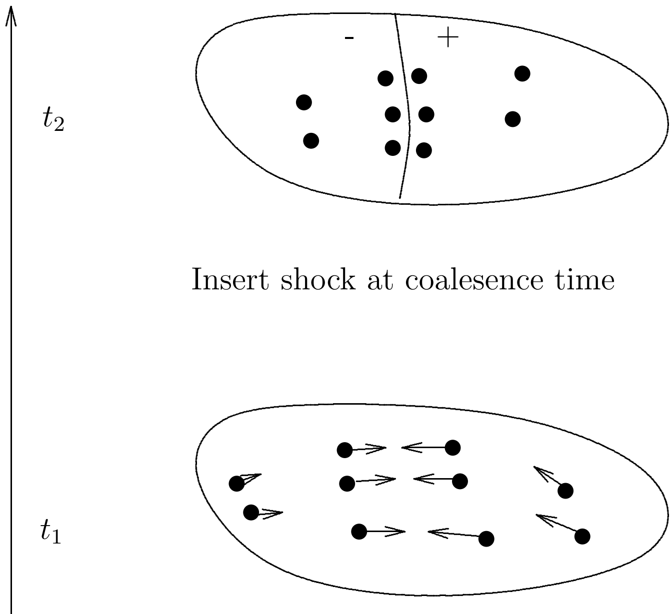

Figure 5: Insertion of shock when knots coalesce.

Consider two distinct knots $\mathbf{x}_a$ and $\mathbf{x}_b$ with corresponding knot velocities $\mathbf{v}_a$ and $\mathbf{v}_b$. If the magnitude of $\mathbf{v}_b$ is small relative to $\mathbf{v}_a$ and $\mathbf{x}_a$ is approaching $\mathbf{x}_b$, then at some time t the two sets of knots are likely to coincide. Without modifying the physics described by the PDEs and boundary conditions, we insert a discontinuous surface at the time of coincidence that splits a continuous subdomain into two new piece-wise continuous subdomains.

Because the knots will move towards high gradient regions, there is the possibility that flat parts of the domain may be too sparsely represented. We interpolate to new knot locations if necessary, or else add or delete knots.

5.5 Maintaining Strict Conservation

Assume that in Ω there are N knots, and assume that we wish to add, delete, or rearrange the knots. First, we must calculate the extensive quantities corresponding to each U_k given by Λ_k where

$$\Lambda_k = \sum_{j=1}^{N+K} \left[\int_\Omega \psi(\mathbf{x} - \mathbf{x}_j) d\mathbf{x} \right] \sigma_{j,k}.$$

Second, we will interpolate the dependent variables U_k onto or into a new set of N_1 knots $\mathbf{y}$. Third, we construct a new set of generalized basis functions ψ, and find the new set of expansion coefficients corresponding to the new set of U_ks. Fourth, we construct a new set of integrals over Ω to minimize the discrepancy between the old integrals and the new integrals

$$\left(\sum_{j=1}^{N_1+K} \left[\int_\Omega \psi(\mathbf{y} - \mathbf{y}_j) d\mathbf{y} \right] \sigma_{j,k} - \Lambda_k \right)^2 \leq \epsilon$$

by adjusting the new $N_1 + K$ expansion coefficients. Most standard Lagragian schemes are concerned primarily with strict mass conservation, but the conservation of the momentum components and total energy are similarly important.

5.6 Shock Wave Collisions

According to Toro [37], shocks that collide normally with other shocks, rarefactions, or contact surfaces are essentially one-dimensional collisions for which the Riemann solver produces the correct set of outgoing waves. These nonlinear outgoing waves might be either a shock or a rarefaction wave depending on the upstream and downstream conditions. Across a contact discontinuity, the velocity and pressure are constant; only the density jump requires a jump in temperature. Therefore this type of solution cannot be observed in isothermal processes.

On the other hand, when dealing with the reflection or collision of oblique waves the problem becomes more complex. In the case of steady oblique shock waves the flow streamlines can intersect the surface of such shock waves at any angle, and in doing so the flow is refracted, i.e. the tangential component of the flow velocity is unchanged while the normal component is diminished. Thus the streamlines are always refracted in a definite direction while passing through an oblique shock wave. The motion behind a shock may be either subsonic or supersonic (only the normal velocity component needs to be less than the velocity of sound); the motion in front of it is necessarily supersonic. In this sense, at an oblique shock, the flow changes direction, so that there are three directions, namely those of the upstream, downstream, and that of the shock itself (for details see P. A. Thompson [36]).

A hodograph plane representation of the velocity components parallel and perpendicular to the flow downstream of an oblique shock is usually called shock polar or Stropkoid curve that represents all possible downstream velocities for a given upstream condition. The polar diagram is obtained from the continuous and discontinuous behavior of the tangential and normal components of the fluid velocity field and the general shock jump conditions. The resulting plot is a cubic curve and every point on the curve represents a possible terminus for the downstream velocity. The basic patterns found at a shock reflection or intersection are: (1) the regular reflection, consisting of an incident, (2) the reflected shock, and (3) the Mach reflection, containing Mach shock and a vortex sheet. A section of a Mach shock is a Mach stem and the one of a vortex sheet is a slip line. The incident, reflected, Mach stem and slip line meet at a triple point. This pattern allows a Mach stem of any length, including zero, and so includes regular reflection as a special case. A complete discussion of the polar diagram and its use is given in C. J. Chapman [10].

As in the case of the head on collision, the intersection of oblique shocks defines a new two-dimensional Riemann problem whose resulting pattern becomes more complex than those observed on a simple head-on collision. The analysis of the resulting flow configuration can be obtained from the pressure-deflection shock polars (see C. J. Chapman [10]). The match between the upstream and downstream flow conditions can be determined from our numerical algorithm. By rotating the governing equations into the direction of principal momentum at each side of the shock and using the Galilean translation transformation, it is found that the resulting interaction appears to be weaker than the one corresponding to the original Eulerian coordinates. Consequently, in this way the analysis of the corresponding Riemann problem in the new reference system becomes simpler.

5.7 Moving Knot Velocities with the Volume Integral Formulation

We initialize the time advanced calculations by constructing the fluxes at each knot within a subdomain from the dependent variables. Suppose we have a Cartesian coordinate system, then using (3), we construct the fluxes along the unit vectors **i**, **j**, **k**. Combining these fluxes via (2) the components of the ℓ-th ($\ell = 1, \ldots, 5$) moving frame velocity vector for an interior knot $\mathbf{x}_i$ are given simply by

$$\left(M\mathcal{F}_\ell(\mathbf{x}_i) - \sum_{k=1}^{M} \mathcal{F}_\ell(\mathbf{x}_k) \right) - \mathbf{v}_\ell(\mathbf{x}_i) \left(MU_\ell(\mathbf{x}_i) - \sum_{k=1}^{M} U_\ell(\mathbf{x}_k) \right) = 0.$$

For the knot velocity components along the boundary, we merely choose a knot on the boundary, and subtract the contributions of the remaining $M-1$ contributions of the flux components and dependent variables. After all the local rotation angles are determined, we also rotate the knot velocity vector so that it is parallel to the principal velocity vector, and we use the relation (10) to construct the characteristic velocities.

6 Solution methods for large RBF systems

The problem of ill-conditioned large systems of equations is not unique to RBFs. Compactly supported methods such as finite differences, finite elements, and finite volumes also suffer from ill-conditioning when the rank of the system becomes very large. However, the ill conditioning grows slower than with global RBF. There are basically four ways to overcome the ill-conditioning problems, see Smith, Bjørstad, and Gropp [35]: (1) pre-conditioning, (2) domain decomposition methods (DDM) using overlapping or non-overlapping schemes, (3) combinations of domain decomposition and preconditioning, and (4) removal of singularities by Pade-contour integration developed by Fornberg and co-workers [20, 21, 22].

Beatson, Cherrie, and Mouat [3] recast the RBFs in terms of a set of basis functions that are discretized solutions of $\Delta^k\phi$. This results in approximate cardinal functions and lowers the computational cost of solving the RBF interpolation problem to $\mathcal{O}(N\log N)$ operations. Interested readers can find more studies of cardinal functions of MQ by Buhmann and Micchelli [9], and Baxter [1]. Another important work of Beatson and co-workers [4, 5, 3, 7] is the fast matrix-vector product algorithm. The set up cost is only $\mathcal{O}(N\log N)$. The evaluation of the MQ expansion at any $\mathbf{x}\in\mathbb{R}^d$ costs $\mathcal{O}(\log N)$ operations that is much faster than the $\mathcal{O}(N)$ operations for direct evaluation. This greatly improves the efficiency of all iterative methods designed for MQ interpolation problems. Mouat [33] showed the condition number for the preconditioned MQ interpolation matrix with 3200 scattered centers in $\mathbb{R}^3$ is of order $\mathcal{O}(10^2)$, whereas that of the unpreconditioned matrix is of order $\mathcal{O}(10^8)$. Recently, Baxter [2] employed the well developed Toeplitz theory into another iterative solver for gridded data. On such data, the resulting matrix would enjoy (block) Toeplitz structure. The inverse of the (MQ) interpolation matrix is constructed by the inverse of its m-by-m principle matrix. In the same paper, a problem with $N = 32768$ and $m = 9$ is solved with the conjugate gradient method.

With Gaussian elimination methods, ill-conditioning grows with the rank of the system of equations, and the number of operations required is proportional to $\mathcal{O}(N^3)$. However, if the domain is decomposed into many semi-independent subdomains containing $N_k \ll N$ points, the condition number in each subdomain is considerably reduced as well as the operation count. At present, we know that geometrical domain decomposition, preconditioning, or a combination of preconditioning and domain decomposition work very effectively for RBF systems (see the papers of Beatson et al. [3, 5, 6, 4], Kansa and Hon [27], and Hon, and Wu [25]).

Although the domain with multiple shocks, contact surfaces, and rarefaction fans are a natural way to decompose the domain physically, we may also decompose the physical subdomains by geometric domain decomposition in such a manner consistent with the concept of load balancing. Combining geometric domain decomposition with preconditioning permits fast iterative solutions rather than those based upon Gaussian elimination.

The volume integral formulation requires a more complex preconditioning scheme. Such a preconditioner will need to be a product form pre-conditioner that is constructed as

$$\mathbf{P} = \mathbf{P}_{interior} \cdot \mathbf{P}_{boundary},$$

where $\mathbf{P}_{boundary}$ operates on the matrix elements of $\mathbf{A}$ associated with the boundary knots, and $\mathbf{P}_{interior}$ operates on the matrix $\mathbf{A}$ associated with the interior knots. Each such preconditioner produces approximate cardinal functions that decay similarly.

Larsson and Fornberg [29] solved elliptic PDEs in the limit of increasingly flat RBFs with relatively few knots and errors $\mathcal{O}(10^{-11})$. Fornberg, Wright, and Larsson [22] have observed that increasingly flat RBFs have a multivariate polynomial as their limit. Also, the existence of the limit depends critically on the knot distribution, and the limit of increasingly flat Gaussians exists regardless of the knot distributions.

With regard to the solutions of PDEs using RBFs, it is foolhardy to assume that straightforward Gaussian elimination methods are suitable on the basis of the operation count and the ill-conditioning problem. The optimal approach will most likely be some hybrid combination of the methods presented in this brief survey.

7 Summary

The purpose of this paper is to formulate a finite volume analog of the meshless radial basis function method for the solution of systems of nonlinear time dependent partial differential equations. The main points of this paper are:

1. We employ physical domain decomposition over piece-wise continuous subdomains that are bounded by shocks, contact surfaces, or rarefaction fans.

2. By a series of rotational and translational transformations, we have converted the set of nonlinear multi-dimensional PDEs into a set of ODEs.

3. The PDEs are applicable at boundaries and boundary conditions are treated as auxiliary constraints to the PDEs.

4. We introduce an additional local transformation that maps these ODEs into compatibility or eigenvector ODEs that propagate at "characteristic" velocities, thereby decoupling the compatibility ODEs.

5. By writing the compatibility variables as a series expansion of RBFs with time dependent expansion coefficients, the time-advanced problem is converted into a method of lines problem. The time-integration is performed to arbitrarily high order.

6. To ensure strict conservation of mass, momentum components, and total energy, we volumetrically integrate the RBFs over the interior of physical subdomains and bounding surfaces. The advantage is not only strict conservation but we obtain higher order convergence since integration (anti-differentiation) is a smoothing process.

7. The volume integration of the RBFs is performed in parallel by integrating over each subdomain Ω_i separately, and normalizing the results. The integration along the boundary surface can also be performed in a parallel manner.

8. We track strong shocks, capture weak shocks using artificial viscosity methods to dampen them, and use Riemann solvers and shock polar methods for shock wave interactions.

9. We have the ability to detect shock formation by monitoring knot distances and velocities. When pairs of knots coincide, we introduce a discontinuous surface at the coincidence loci. We add, delete, or rearrange knots within a physical subdomain by a volume integral interpolation analog that maintains strict conservation.

10. We introduce higher order preconditioners and geometric domain decomposition to solve the systems of equations by iterative methods rather than by Gaussian elimination.

11. Various one and two dimensional propagating shock wave problems will be presented with the volume integral RBFs in a forthcoming paper.

8 Appendix. Indefinite Multiquadric Integrals in One, Two, and Three Dimensions

8.1 Preliminaries of Integrating the MQ Basis Functions

In order to simplify the notation, it shall be understood that we deal only with RBFs centered at $(x_j, y_j, z_j) = (0,0,0)$. We shall begin with the popular multiquadric radial basis function given by

$$\phi(\mathbf{x}) = \sqrt{x^2+y^2+z^2+c^2}.$$

8.1.1 One Dimensional Integrals

This integration is performed by holding y and z fixed, and integrating over x, yielding:

$$\int \phi(\mathbf{x})dx = \frac{x}{2}\phi(\mathbf{x}) + \frac{c^2+y^2+z^2}{2}\log(\phi(\mathbf{x})+x) + C_1. \tag{14}$$

8.1.2 Two Dimensional Integrals

This integration is performed by holding x and z fixed in (14), and integrating over y. These integrals were performed with Mathematica by Prof. C. Y. Chan and Prof. A. Cheng, and rechecked by differentiating.

The indefinite integral of the MQ-RBF over x and y is

$$\begin{aligned}\int\int \phi(\mathbf{x})dxdy \quad &= \quad \frac{xy\phi(\mathbf{x})}{3} + \frac{3x(c^2+z^2)+x^3}{3}\log\left(\phi(\mathbf{x})+y\right) \\ &+\frac{3y(c^2+z^2)+y^3}{3}\log\left(\phi(\mathbf{x})+x\right) - \frac{y(c^2+z^2)}{3} - \frac{y^3}{18} \\ &-\frac{\sqrt[3]{c^2+z^2}}{6}\arctan\left(\frac{y\sqrt{c^2+z^2}}{x\phi(\mathbf{x})+x^2+z^2+c^2}\right).\end{aligned}$$

8.1.3 Three Dimensional Integrals

The next step is the integration over the variable z:

$$
\begin{aligned}
&\int\int\int \phi(\mathbf{x})dxdydz = \\
&\frac{xyz\phi(\mathbf{x})}{3} - \frac{xz(6c^2+z^2)}{18} - \frac{yz(12c^2+y^2+3z^2)}{18} \\
&+\frac{yz(3c^2+y^2+z^2)}{6}\log\left(\phi(\mathbf{x})+x\right) + \frac{xz(3c^2+x^2+z^2)}{6}\log\left(\phi(\mathbf{x})+y\right) \\
&+\frac{2xyc^2}{3}\log\left(\phi(\mathbf{x})+z\right) + \frac{yc^2\sqrt{y^2+c^2}}{3}\arctan\left(\frac{z\sqrt{y^2+c^2}}{x^2+y^2+c^2+x\phi(\mathbf{x})}\right) \\
&+\frac{xc^2\sqrt{x^2+c^2}}{3}\arctan\left(\frac{z\sqrt{x^2+c^2}}{x^2+y^2+c^2+y\phi(\mathbf{x})}\right) \\
&+\int\frac{\sqrt[3]{(z^2+c^2)}}{3}\arctan\left(\frac{y\sqrt{z^2+c^2}}{x\phi(\mathbf{x})+x^2+z^2+c^2}\right)dz.
\end{aligned}
$$

The integration of the last term does not appear to give a closed form solution. An alternative is to use Gauss-Legendre intergation over the variable z.

8.2 Volumetric Gaussian Integrals

The volume integrals of Gaussian RBFs are simple

$$\int\int\int e^{-c^2(x^2+y^2+z^2)}dxdydz = \frac{\pi^{3/2}}{8c^3}\mathrm{erf}(cx)\mathrm{erf}(cy)\mathrm{erf}(cz).$$

9 Acknowledgements

We wish to thank Prof. C. Y. Chan and Prof. Alexander Chang for their help with Mathematica in constructing the two and three dimensional indefinite integrals of the multiquadric basis functions.

References

[1] B. Baxter, The asymptotic cardinal function of the multiquadratic $\phi(r) = (r^2 + c^2)^{1/2}$ as $c \to \infty$. Comput. Math. Appl. **24**(12): 1-6 (1992).

[2] B. Baxter, Preconditioned conjugate gradients, radial basis functions, and Toeplitz matrices. Comput. Math. Appl. **43**(3-5): 305-318 (2002).

[3] R. K. Beatson, J. B. Cherrie, and C. T. Mouat, Fast fitting of radial basis functions: Methods based on preconditioned GMRES iteration. Adv. Comput. Math. **11**: 253-270 (1999).

[4] R. K. Beatson, J. B. Cherrie, and G. N. Newsam, Fast evaluation of radial basis functions: methods for generalized multiquadrics in $\mathbb{R}^n$. SIAM J. Sci. Comput. **23**(5): 1549-1571 (2002).

[5] R. K. Beatson, and W. A. Light, Fast evaluation of radial basis function: methods for two-dimensional polyharmonic splines. IMA Journal of Numerical Analysis, **17**: 343-372 (1997).

[6] R. K. Beatson, W. A. Light, and S. Billings, Fast solution of the radial basis function interpolation methods: Domain Decomposition Methods. SIAM J. Sci. Comput. **22**(5): 1717-1740 (2000).

[7] R. K. Beatson, and G. N. Newsam, Fast evaluation of radial basis functions: I. Computers Math. Applic., **24**,(12): 7-19 (1992).

[8] R. B. Bird, W. E. Stewart and E. N. Lightfoot, *Transport Phenomena*, John Wiley and Sons, NY (1960).

[9] M. D. Buhmann, and C. A. Micchelli, Multiquadric interpolation improved. Comput. Math. Appl. **24**(12): 21-25 (1992).

[10] C. J. Chapman, *High speed flow*, Cambridge texts in applied mathematics, Cambridge University Press, Cambridge (2000).

[11] J-S. Chen, C. T. Wu, S. Yoon, and Y. You, A stabilized conforming nodal integration for Galerkin mesh-free methods, Int. J. Numer. Meth. Eng. **50**: 435- 466 (2001).

[12] J-S. Chen, S. Yoon, and C. T. Wu, Non-linear version of stabilized conforming nodal integration for Galerkin mesh-free methods, Int. J. Numer. Meth. Eng. **53**: 2587-2615 (2002).

[13] W. Chen and J. He, A study on radial basis function and quasi-Monte Carlo methods, Int. J. Nonlinear Sci. & Numer. Simulation, **1**(4): 343-342, (2000).

[14] W. Chen, New RBF collocation schemes and kernel RBFs with applications, Lecture Notes in Computational Science and Engineering, **26**: 75-86, (2002).

[15] W. Chen, Symmetric boundary knot method, Engng. Anal. Bound. Elem., **26** (6): 489-494, (2002).

[16] W. Chen, Distance function wavelets - Part III: "Exotic" transforms and series, Research report of Simula Research Laboratory, CoRR preprint, June, (2002).

[17] I.-L. Chern, J. Glimm, O. McBryan, B. Plohr, and S. Yaniv, Front tracking for gas dynamics, J. Comput. Phys., **62**: 83-110 (1986).

[18] C. K. Chui, J. Stöckler, and J. W. Ward, Analytic wavelets generated by radial functions, Adv. Comput. Math **5**: 95-123 (1996).

[19] H. Deconinck, Ch. Hirsch, and J. Peutman, Characteristic decomposition methods for the multidimensional Euler equations, *Lecture Notes in Physics, Volume 274*, Springer Verlag, New York (1986).

[20] B. Fornberg and T. A. Driscoll, Interpolation in the limit of increasingly flat radial basis functions. Comput. Math. Applic. **43**(3-5): 413-421 (2002).

[21] B. Fornberg and G. Wright, Stable computation of multiquadric interpolants for all values of the shape parameter. BIT (to appear).

[22] B. Fornberg, G. Wright, and E. Larsson, Some observations regarding interpolants in the limit of flat radial basis functions, Comput. Math. Applic. (submitted, 2002).

[23] R. Franke, Scattered data interpolation: tests of some methods, Math. Comput. **98**: 181-200 (1982).

[24] J. Glimm, J. W. Grove, X.-L. Li, K.-M. Shyue, Q. Zhang, and Y. Zeng, Three dimensional front tracking, SIAM J. Sci. Comp. **19**: 703-727 (1998).

[25] Y. C. Hon, and Z.Wu, Additive Schwarz domain decomposition with radial basis approximation. Int. J. Appl. Math. **4**: 81-98 (2002).

[26] E. J. Kansa, Local, point-wise rotational transformations of the conservation equations into stream-wise coordinates. Comput. Math. Applic. bf 43(3-5): 501-511 (2002).

[27] E. J. Kansa and Y. C. Hon, Circumventing the ill-conditioning problem with multiquadric radial basis functions: Applications to elliptic partial differential equations. Comput. Math. Applic. bf 39(7/8): 123-137 (2000).

[28] C. B. Laney, *Computational Gas Dynamics*. Cambridge University Press, Cambridge, UK (1998).

[29] E. Larsson and B. Fornberg, A numerical study of radial basis functions based solution methods for elliptic pdes. Comput. Math. Applic. (to appear).

[30] W. R. Madych and S. A. Nelson, Multivariate interpolation and conditionally positive definite functions, II, Math. Comput. **54**: 211-230 (1990).

[31] N. Mai-Duy and T. Tran-Cong, Numerical solution of differential equations using multiquadric radial basis function networks. Neural Networks **14**: 185-199 (2001).

[32] N. Mai-Duy and T. Tran-Cong, Numerical solution of Navier-Stokes equations using multiquadric radial basis function networks. Int. J. Num. Meth. Fluid **37**: 65-86 (2001).

[33] C. T. Mouat, Fast algorithms and preconditioning techniques for fitting radial basis functions. Ph.D. thesis, Mathematics Department, University of Canterbury, Christchurch, New Zealand (2001).

[34] R. Schaback, On the efficiency of interpolation by radial basis functions, in *Surface Fitting and Multiresolution Methods*, A. Le Méhauté, C. Rabut, and L. L. Schumaker (eds.), Vanderbilt University Press (Nashville TN): 309-318 (1997).

[35] B. F. Smith, P. E. Bjørstad, and W. D. Gropp, *Domain Decomposition: Parallel Multilevel Methods for Elliptic Partial Differential Equations*, Cambridge University Press, Cambridge, UK (1996).

[36] P. A. Thompson, *Compressible fluid dynamics.* McGraw-Hill Book Co., New York (1972).

[37] E. F. Toro, *Riemann solvers and Numerical methods for fluid dynamics.* Springer-Verlag, Berlin (1999).